Bulletin of the Seismological Society of America, Vol. 99, No. 4, pp. 2169–2179, August 2009, doi: 10.1785/0120080324

Analysis of the Tsunami Generated by the Great 1977 Sumba Earthquake that Occurred in Indonesia

by Aditya R. Gusman, Yuichiro Tanioka, Hiroyuki Matsumoto, and Sin-Iti Iwasaki

Abstract The great outer-rise earthquake (M_w 8.3) occurred near the Sunda trench, Indonesia, on 19 August 1977. The earthquake has been previously studied using seismological data. The earthquake generated a large tsunami that caused severe damage in Sumbawa and Sumba Islands in Indonesia. The tsunami was also observed at tide gauges in Australia. We numerically computed a far-field tsunami, and we compared the observed tsunami waveforms on three tide gauges with the computed waveforms. We also numerically computed the tsunami inundation and compared the observed tsunami run-up of 8 m and tsunami inundation distance of 500 m in Lunyuk on Sumbawa Island with the computed ones. To explain the observed tsunami waveforms, tsunami run-up, and tsunami inundation distance, the slip amount is found to be 3 m on the assumed fault model (with a fault length of 200 km and fault width of 70 km). The rigidity is assumed to range between 6.0 and 6.8×10^{10} N m^{-2}, and the range of the total seismic moment is calculated to be between 2.5 and 2.9×10^{21} N m (M_w 8.2), which is similar to those estimated by the previous seismological studies. Additionally, we calculated the ratio between the observed tsunami run-up and the computed maximum tsunami height along the coastline of Lunyuk. This ratio, called the amplification factor, may possibly be used to roughly estimate the tsunami run-up from a tsunami numerical calculation result on a coarse grid system.

Introduction

A large earthquake with a moment magnitude of M_w 8.3 occurred off the southwest coast of Sumba Island, Indonesia. The location of the epicenter is 11.16° S–118.41° E, with an origin time of 06:08:54.8 universal coordinated time (UTC) (14:08:54.8 local time) on 19 August 1977 (Lynnes and Lay, 1988). The epicenter of this earthquake was located near the Sunda trench of the Lesser Sunda subduction zone (Fig. 1). The seismic moment of the great 1977 Sumba earthquake estimated from seismological analysis ranges from 2.4 to 4.0×10^{21} N m (M_w 8.2–8.3) (Given and Kanamori, 1980; Silver and Jordan, 1983; Giardini *et al.*, 1985). The relocated aftershocks along the trench extend about 130 km eastward and 110 km westward from the epicenter (Spence, 1986). The aftershock area and surface wave results of Zhang and Kanamori (1988) imply a total length of the fault that is at least 200 km. The waveform analysis of the teleseismic body wave indicated a total length of 200 km, extending to 35–50 km in depth (Lynnes and Lay, 1988). Given and Kanamori (1980) obtained the focal mechanism of the earthquake using surface waves (strike = 270°, dip = 45°, and rake = −70°) (Fig. 1). The great 1977 Sumba earthquake is the biggest outer-rise earthquake in Indonesia ever recorded. The mechanism of outer-rise events is generally a normal fault type with the tension axis perpendicular to the trench, and the focal depths are quite shallow. These aspects are basically consistent with the bending lithosphere interpretation (Chapple and Forsythe, 1979). Another interpretation is that before a major underthrusting earthquake, the interplate boundary is strongly coupled, the down-dip slab is under tensional stress, and the outer-rise region is under compressional stress. After a major underthrust earthquake ruptures the plate interface, the outer-rise region is under tensional stress, whereas the down-dip slab may be either under compression or under diminished tensional stress (Astiz *et al.*, 1988). Ruff (1996) shows that the largest outer-rise events have tensional focal mechanisms, and they tend to occur in uncoupled subduction zones, for example, the 2 March 1933 Sanriku (M_w 8.4) and 19 August 1977 Sumba (M_w 8.3) events.

The tsunami generated by the earthquake caused severe damage in the Indonesian islands, and it was also witnessed in Australia. A post-tsunami survey team was assembled right after the event. They visited four islands in Indonesia: Bali, Lombok, Sumbawa, and Sumba Islands. The survey team measured 17 tsunami run-up heights (International Tsunami Information Center [ITIC], 1977). The highest tsunami estimated from eyewitness account was 8 m and the inundation distance was 500 m at Lunyuk on Sumbawa Island.

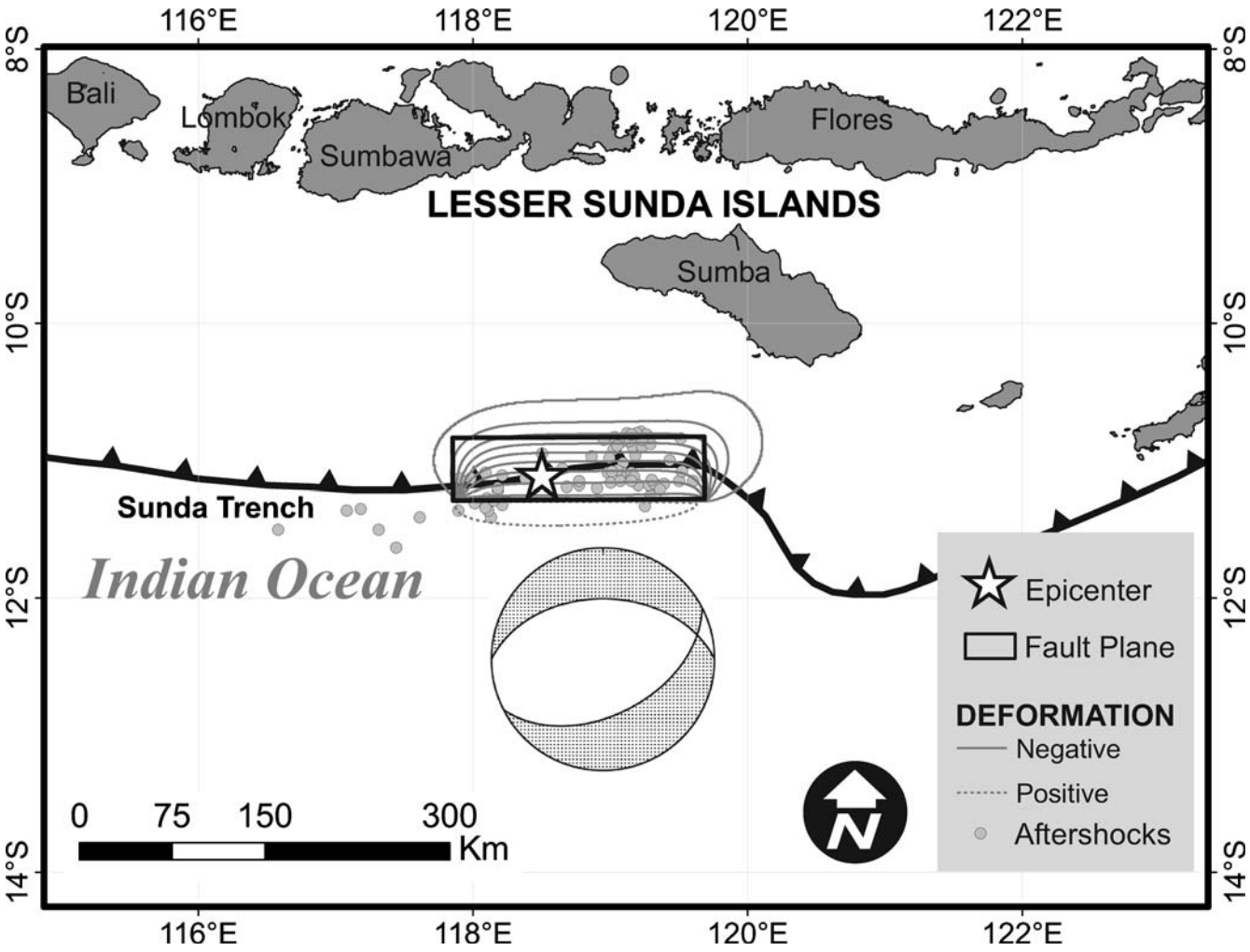

Figure 1. Tectonic settings near the source region of the 1977 Sumba earthquake. Contours show the vertical crustal deformation calculated from the best fault model. Solid contours are the negative deformation and dashed contours are the positive deformation. The contour interval is 0.2 m. The focal mechanism of the earthquake obtained by Given and Kanamori (1980) that is used in this study is also shown. The rectangular box shows the location of the fault that we used for tsunami computation; the fault plane is dipping to the north, the fault length is 200 km, and the width is 70 km. The star is the epicenter of the 1977 earthquake, and the gray circles are aftershocks recorded by the U.S. Geological Survey (USGS) and the International Seismological Centre (ISC).

Another high tsunami run-up of 5.5 m with the inundation distance of 1200 m was observed at Leterua on Sumba Island. The summary of tsunami heights measured by the team is shown in Table 1 (ITIC, 1977; Kato and Tsuji, 1995). Kato and Tsuji (1995) also observed that the earthquake was associated with strong ground motion. People in Australia felt a strong shake and went outside the buildings, while people in the affected tsunami area reported an unusual explosion after the earthquake. The island most damaged by the tsunami waves was Sumbawa Island, where 68 people were killed and 54 people were missing. The combined number of victims from both the earthquake and tsunami in Indonesia was 107 people.

The great 1977 Sumba earthquake was one of the rare outer-rise earthquakes that occur near subduction interfaces that generate big tsunamis. The most recent event was the 2007 earthquake (M_w 8.1) that occurred near the central Kuril Islands. According to the tsunami numerical simulation conducted by Robinovich *et al.* (2008), the calculated maximum tsunami generated by the 2007 earthquake is larger than that generated by the 2006 great interplate earthquake (M_w 8.3) that occurred in a same region. However, the area impacted by the higher waves of the 2007 event was very local. Because seafloor deformations associated with these earthquakes often occur in deep water, for a given seismic moment, there is more shoaling amplification of the tsunami compared with typical subduction zone earthquakes that occur beneath shallower water. It is important to emphasize that the tsunami generation from these great outer-rise earthquakes is not presently included in real-time tsunami forecasting systems (Titov *et al.*, 2005).

In this article, we chose a focal mechanism and a fault dimension for this earthquake that was obtained by seismological analysis from previous studies. We estimate the slip

Table 1

Tsunami Height Measured by ITIC Team with Damage and Inundation Remarks

Island	Location	Heights (m)	Remarks
Bali	Nusa Dua (8°48′ S, 115°13′ E)	2.5	No damage
		4.0	
	Benoa (8°46′ S, 115°23′ E)	1.5	No damage
Lombok	Labuanhaji (8°35′ S, 116°33′ E)	3.2	Inundation 100 m; fishing boats were wrecked; one person was killed
		4.1	
		3.8	
	Awang (8°55′ S, 116°24′ E)	4.0	Inundation 200 m; fishing boats were wrecked; trees were uprooted; houses were destroyed; 20 people were killed
		2.0	
		4.3	
	Batunampar (8°51′ S, 116°24′ E)	2.0	No damage
	Kuta (8°53′ S, 116°12′ E)	4.3	Inundation 100 m; fishing boats were wrecked; one person was killed
		5.5	
Sumbawa	Lunyuk (9°02′ S, 117°10′ E)	5.8	Inundation 500 m; 65 people were killed and 37 were missing
Sumba	Leterua (9°46′ S, 119°12′ E)	5.5	Inundation 1200 m
		4.8	
	Melolo (9°56′ S, 120°45′ E)	1.5	Small damage on houses
	Waingapu (9°38′ S, 120°16′ E)	1.0	No damage

amount using tsunami waveform analysis by comparing the observed tsunami waveforms at a tide gauge with simulated ones. Using the tsunami inundation model, we also examine fault models to explain the observed tsunami run-up and inundation in Lunyuk, Sumbawa. We also calculate the amplification factor for Lunyuk Bay, which can be used to roughly estimate tsunami run-up using a simple tsunami numerical simulation with a low resolution grid system.

Data and Method

The tsunami generated by the great 1977 Sumba earthquake was recorded by three tide gauge stations in Australia. A survey team also measured the tsunami inundation distance and run-up in Lunyuk, Sumbawa. We use three tsunamis recorded on tide gauges in Australia for comparison of the observed tsunami waveforms with the computed ones. The reported tsunami inundation and run-up data are used for comparison with the computed inundation and run-up.

The following steps are taken for the tsunami analysis. First, we choose the focal mechanism estimated by previous studies using the seismological data. The length and width of the fault model are derived from previous studies (Lynnes and Lay, 1988; Zhang and Kanamori, 1988), along with the aftershock distribution of the earthquake. Finally, we estimate the slip amount by fitting the tsunami amplitude recorded at the tide gauge with the simulated ones and also fitting the tsunami run-up and inundation data at Lunyuk, Sumbawa, with the simulated ones.

Far-Field Tsunami

In Indonesia, there were no tide gauge records for the tsunami, but the tsunami was recorded by tide gauges located in Australia. Three tide gauges in Australia, two tide gauges in Dampier, and one in Port Hedland recorded the tsunami. However, the records have a poor resolution and only one tide gauge showed distinct amplitude (Fig. 2). The record at Port Hampton in the town of Dampier shows a maximum amplitude of 0.8 m on a later phase. We use this record as the main data for the tsunami waveform analysis. Two tide gauges are located at Dampier, the first at the service wharf (Dampier) located at 116°43′40″ E, 20°38′21″ S and a second at the tug jetty (Hampton Harbor) located at 116°41′03″ E, 20°39′50″ S. The tide gauge at the service wharf is in an exposed position while the tide gauge at the tug jetty is within the sheltered and confined waters of Hampton Harbor. The service wharf gauge failed to record between the hours of approximately 17:40 and 17:55 Western Standard Time (WST) (Fig. 2), probably due to the initial surge of water upsetting the instrument. The instrument was noted to have moved slightly (Captain D.W. Nielsen's report, in ITIC, 1977). The third tide gauge is located in Port Hedland, Australia (118°34′ E, 20°19′ S). From the tide gauge records it is clear that the tsunami first arrives at the Australian coastline during low tide. Maybe this is the reason why there was no major damage in Australia from this tsunami.

The bathymetry we use for tsunami numerical simulation is based upon the General Bathymetric Chart of the Oceans (GEBCO) dataset and nautical charts of Dampier, Port Hedland waters, and Alas Strait (between Lombok and Sumbawa Islands). The nautical charts supplied by the National Imagery and Mapping Agency give more accurate bathymetry around Dampier waters where the tide gauges are located. Because the GEBCO dataset has a poor accuracy on shallow water regions, we use bathymetry data digitized from the nautical charts. The grid spacing for the

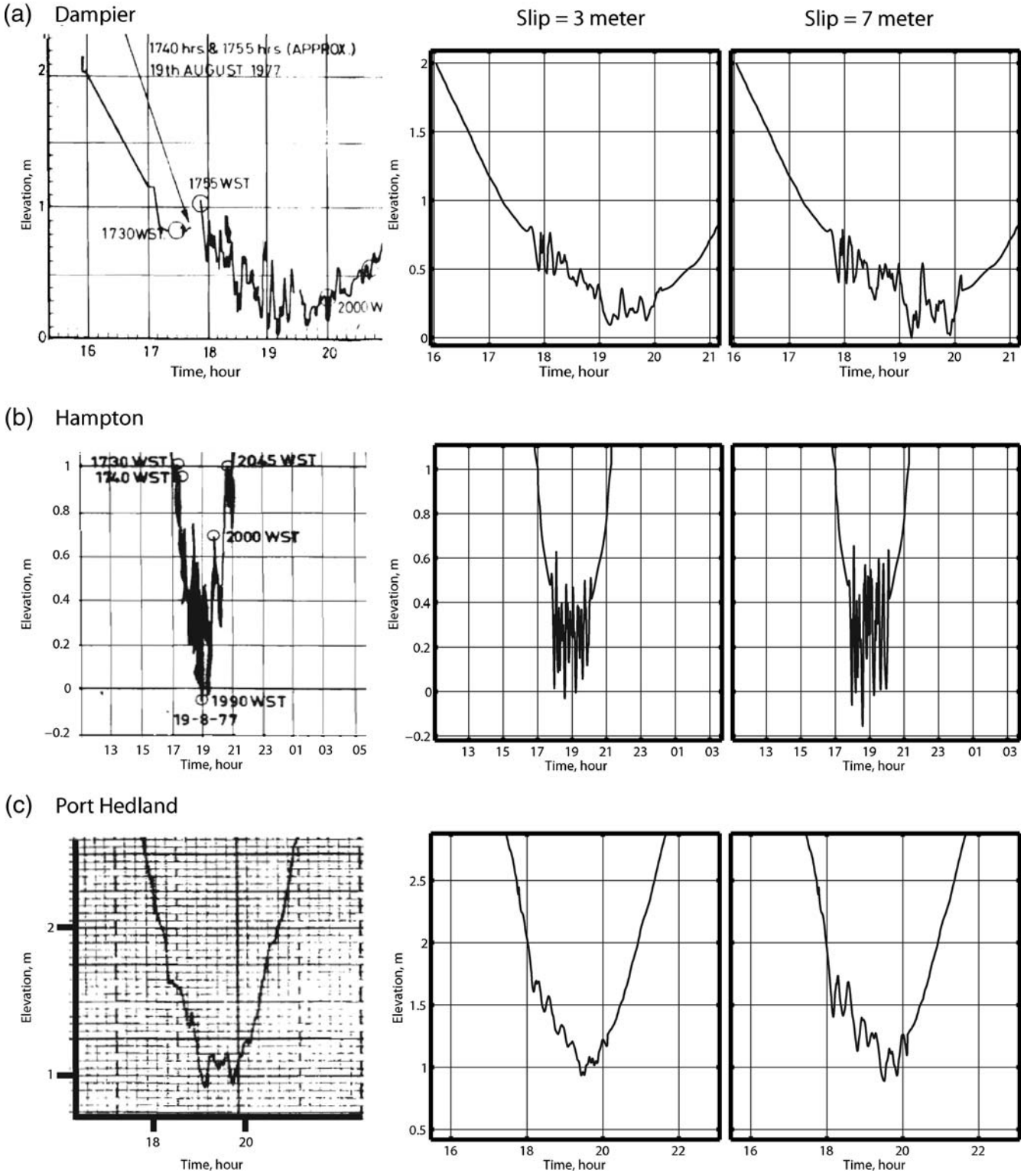

Figure 2. Comparison of recorded (left-hand panels) with computed tsunamis (center and right-hand panels) at Dampier, Hampton, and Port Hedland for the great 1977 Sumba earthquake using the slip amounts of 3 and 7 m on the fault model shown in Figure 1. The locations of the three tide gauges are shown in Figure 3.

numerical simulation that covers all computational areas is 1 arcmin. We use a finer grid near the coastal area around the tide gauge stations; the finest grid system is 6.7 arcsec.

In order to simulate tsunami propagation, initial water surface deformation must be calculated. The water surface deformation due to faulting of a large earthquake is assumed to be the same as the ocean bottom deformation because the wavelength of the ocean bottom deformation is much larger than the ocean depth (Satake, 2002); to use this assumption the wavelength of the ocean bottom deformation (L) has to be much larger than the ocean depth (D) or $D/L < 0.05$. Vertical deformation of the sea floor (Fig. 1) caused by the earthquake is calculated from analytical expressions for the deformation (Mansinha and Smylie, 1971).

The governing equations for the far-field tsunami computation are the following. We take the spherical coordinate system (r, θ, and φ) with the origin at the Earth's center. The Earth is assumed to be a sphere, so r is constant and equal to the Earth's radius R, covered by latitude (θ) and longitude (φ). The shallow water or the long wave theory is given by the following expressions:

$$\frac{\partial \eta}{\partial t} + \frac{1}{R\cos\theta}\left[\frac{\partial M}{\partial \varphi} + \frac{\partial N}{\partial \theta}(\cos\theta)\right] = 0, \tag{1}$$

$$\frac{\partial M}{\partial t} + \frac{1}{R\cos\theta}\left[\frac{\partial}{\partial \varphi}\left(\frac{M^2}{D}\right) + \frac{\partial}{\partial \theta}\left(\frac{MN}{D}\right)(\cos\theta)\right] = fN - \frac{gD}{R\cos\theta}\frac{\partial \eta}{\partial \varphi} - \frac{C_f}{D^2}M\sqrt{M^2+N^2}, \tag{2}$$

and

$$\frac{\partial N}{\partial t} + \frac{1}{R\cos\theta}\left[\frac{\partial}{\partial \varphi}\left(\frac{MN}{D}\right) + \frac{\partial}{\partial \theta}\left(\frac{N^2}{D}\right)(\cos\theta)\right] = -fM - \frac{gD}{R}\frac{\partial \eta}{\partial \theta} - \frac{C_f}{D^2}N\sqrt{M^2+N^2}, \tag{3}$$

where

$$C_f = \frac{gn^2}{D^{1/3}}. \tag{4}$$

The nondimensional frictional coefficient C_f is calculated using Manning's roughness n, which is assumed to have a constant of 0.03. In the equations, t is time, η is the water level, M and N are discharge fluxes along latitude and longitude axes, respectively, g is the gravitational acceleration, D is the total water depth, and f is the Coriolis coefficient. The open boundary condition at the edge of the computational area and the total reflection boundary at the shoreline are used for computation. The tsunami computational area is 109°–126° E and 7°–23° S, which covers most of Lesser Sunda Islands and northern part of western Australia (Fig. 3). A nested grid system is used to ensure continuities between the small region and the large region. A computational time-step of 0.5 sec is chosen to satisfy the Courant–Friedrichs–Lewy stability condition that is expressed by the following equation:

$$\Delta t \le \frac{\Delta x}{\sqrt{2gh}}. \tag{5}$$

The physical meaning of the stability condition is that the timestep Δt must be equal to or smaller than the time required for the wave to propagate the spatial grid size Δx.

A slip amount of the Sumba earthquake is estimated by fitting the observed tsunami records with the simulated ones. In general, comparison of the amplitudes can be done by digitizing the original marigram and removing the tide from the records. Because of the bad quality of the records as shown in Figure 2, tsunami waves on the marigram cannot be digitized correctly. Therefore, we used a scanned marigram for the comparison and tried to fit the waves by adding the tide that was calculated from the original marigram on the simulated tsunami waves.

Tsunami Inundation

For tsunami inundation simulation, we selected Lunyuk Bay on Sumbawa Island (Fig. 4) where the highest tsunami run-up of 8 m was observed and the inundation was extended to 500 m inland. Lunyuk Bay is a small bay that has a size of approximately 16 × 8 km. The deepest water at the mouth of the bay is about 280 m. This indicates that the bay has a slope about 0.035 (Fig. 4). We used nautical charts provided by the Indonesian Navy for bathymetry around Lunyuk Bay and Shuttle Radar Topography Mission (SRTM) data for the topography. For Lunyuk Bay we prepared a finest grid system of 68 m (2 sec) for the tsunami inundation model. Bathymetry or terrain data on all grid points are obtained by interpolation of the nautical chart and 90 m SRTM data, respectively. The exact location of the 8 m run-up and the 500 m inundation is not clear. We suspect that the inundation of 500 m was observed near a present village, on the east side of the river (Fig. 5). We made 12 profiles of the tsunami inundation (Fig. 5) within this area in order to verify the tsunami inundation model with the observation data.

The tsunami run-up heights along the coast of Lunyuk were simulated by solving the nonlinear momentum conservation equation with bottom friction terms. The bottom friction terms in the equation were expressed by analogy to the quadratic friction law in uniform flow (Imamura, 1996). The resulting expression, which is called the shallow water or the long wave theory, in the Cartesian coordinate system is given by

$$\frac{\partial M}{\partial t} + \frac{\partial}{\partial x}\left(\frac{M^2}{D}\right) + \frac{\partial}{\partial y}\left(\frac{MN}{D}\right) + gD\frac{\partial \eta}{\partial x} + \frac{C_f}{D^2}M\sqrt{M^2+N^2} = 0, \tag{6}$$

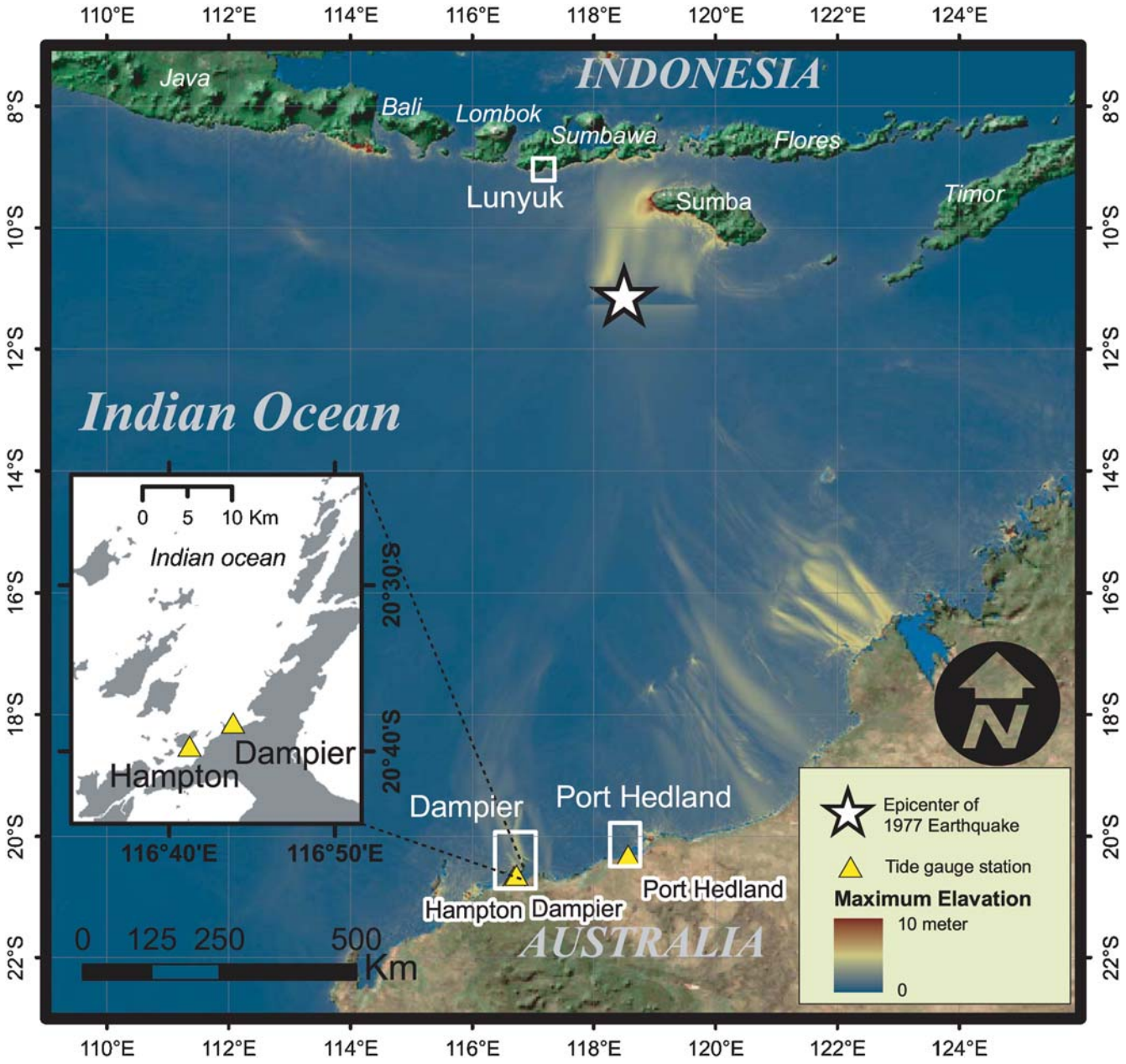

Figure 3. Maximum tsunami elevation calculated from the far-field tsunami simulation. The white rectangles are the computation domains for small grid systems. The tsunami was recorded by three tide gauges located in Australia. Those tide gauges are indicated by yellow triangles. The inset map shows a closer look at the Dampier region where two tide gauges are located.

$$\frac{\partial N}{\partial t}+\frac{\partial}{\partial x}\left(\frac{MN}{D}\right)+\frac{\partial}{\partial y}\left(\frac{N^2}{D}\right)+gD\frac{\partial \eta}{\partial y}+\frac{C_f}{D^2}N\sqrt{M^2+N^2}=0. \quad (7)$$

Most of the parameters used in equations (6) and (7) are the same as those in equations (2) and (3). M and N are the horizontal depth averaged volume flux vectors in the x and y directions, respectively. For the nondimensional frictional coefficient C_f we assume that Manning's roughness n on Lunyuk beach has a constant value of 0.03. Boundary conditions for tsunami run-up computation are determined by the judgment of a cell for being submerged or dry. Discharge across the boundary between two cells is calculated if the ground height in the dry cell is lower than the water level in the submerged cell; otherwise, the discharge is considered to be zero (Imamura, 1996). These are called moving boundary conditions.

Fault Model

Several authors have published focal mechanisms for the 1977 Sumba event. Giardini *et al.* (1985) obtained a centroid moment tensor solution with a best double couple

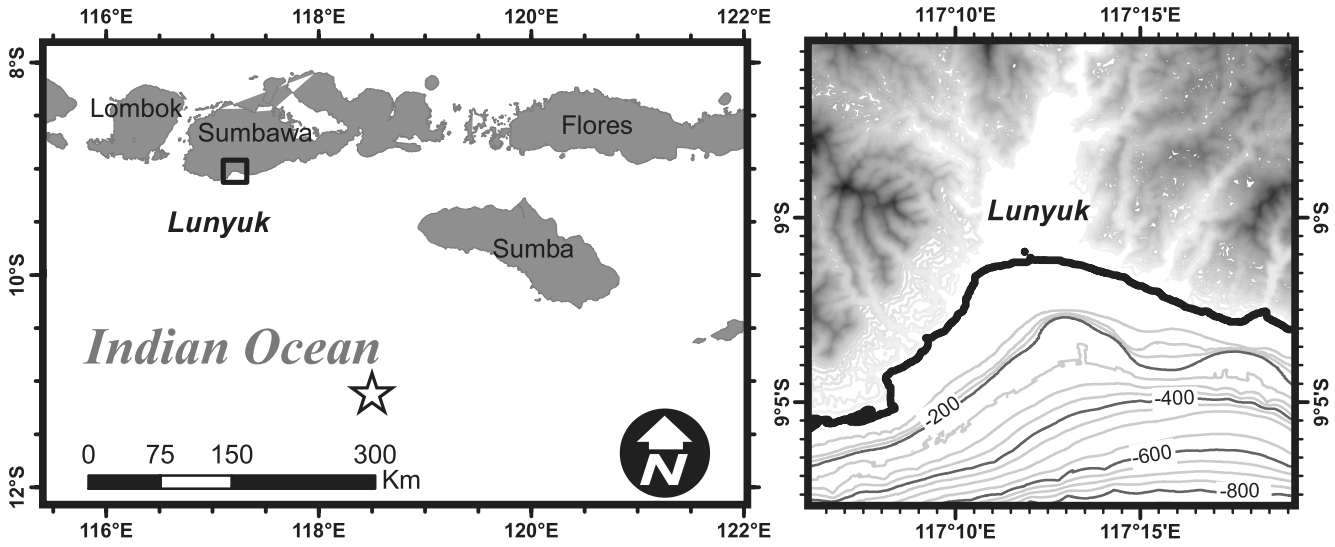

Figure 4. The location of Lunyuk Bay (left-hand panel) and the detailed bathymetry and topography around Lunyuk Bay (right-hand panel). Lunyuk Bay is located on Sumbawa Island 290 km northwest from the epicenter (white star) of the 1977 Sumba earthquake.

(strike = 264°, dip = 24°, and rake = −73°) using a long-period surface wave. Given and Kanamori (1980) obtained a mechanism (strike = 270°, dip = 45°, and rake = −70°) also from long-period waves; and Spence (1986) obtained a similar *P*-wave first motion mechanism (strike = 279°, dip = 45°, and rake = −80°). In this study, we chose the Given and Kanamori (1980) surface wave mechanism. According to Lynnes and Lay (1988), the focal mechanism obtained by Given and Kanamori (1980) represents an average mechanism for the full rupture history and is also compatible with the *P*-wave first motion mechanism obtained by Spence (1986) and the first motions of the phases used in

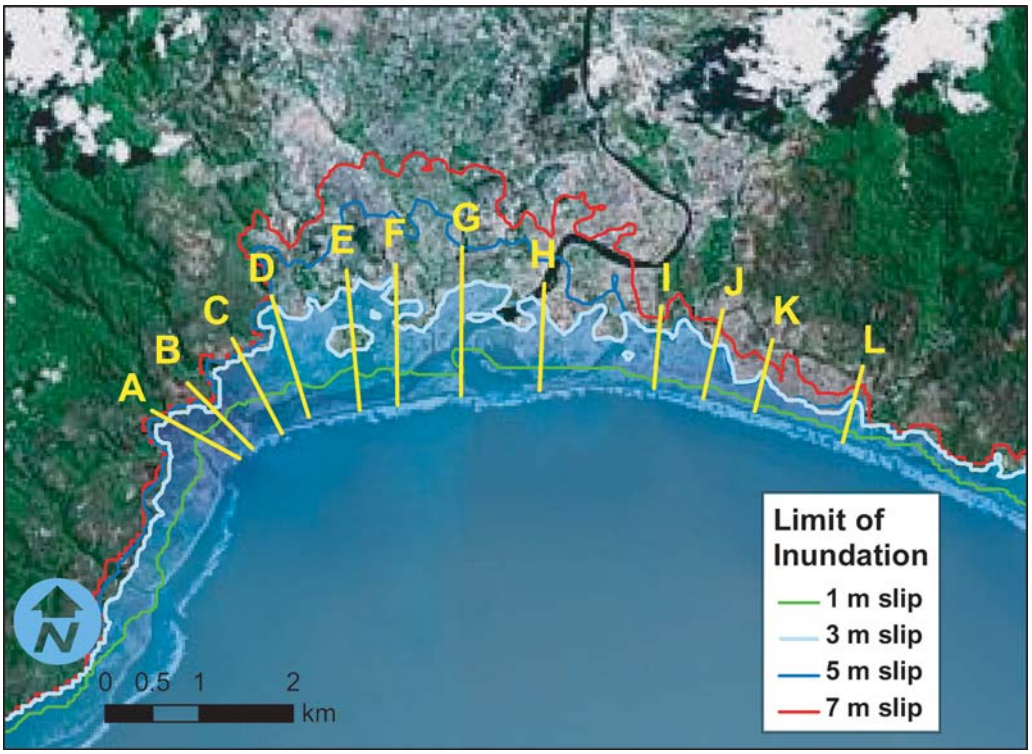

Figure 5. Computed tsunami inundation area overlay with the satellite image of Lunyuk. The 12 yellow lines are for the inundation profiles in Figure 7. The gray line and transparent blue area represent inundation computed from the fault model with the slip amount of 3 m. The red, blue, and green lines represent the limit of inundation computed from the fault model with the slip amounts of 7, 5, and 1 m, respectively.

their study, while the mechanism obtained by Giardini *et al.* (1985) violates some of the *P*-wave first motions.

According to the eyewitness accounts in Lombok, the ocean receded before the tsunami hit the shore (ITIC, 1977). The report of the tsunami in Australia does not show any indication that the sea withdrew prior to the tsunami, so it is most likely that the tsunami in Australia had a positive front (ITIC, 1977). This can only be explained if we use the north dipping fault plane to get the sea surface deformation with a negative front to the north and a positive front to the south (Fig. 1), while the other solution of the focal mechanism will flip the fronts of the sea surface deformation pattern.

We use fault parameters as follows: strike = 270°, dip = 45°, rake = −70° (Given and Kanamori, 1980), length = 200 km, width = 70 km, the coordinates of the southeast corner of the fault plane are 119°41.1′ E–11°16.68′ S, and the shallowest depth of the fault is 1 km (Fig. 1). Lynnes and Lay (1988) indicate that the deepest extend of the earthquake source has a range from 35 to 50 km. Because the dip angle is 45°, the fault width should be between 50 and 70 km. We calculated surface deformations using two fault widths of 50 and 70 km. However, on a given moment magnitude, the computed tsunami waveforms at the tide gauge stations in Australia and the computed tsunami inundation in Lunyuk, Sumbawa, from the two fault models show almost the same tsunami waveform and inundation. In this article, we chose a fault width of 70 km to analyze the tsunami generated by this earthquake.

The previous fault model generates an ocean bottom deformation with a wavelength (L) about 110 km and the deformation located in the ocean with an average depth (D) about 5 km. The ratio between the depth and wavelength

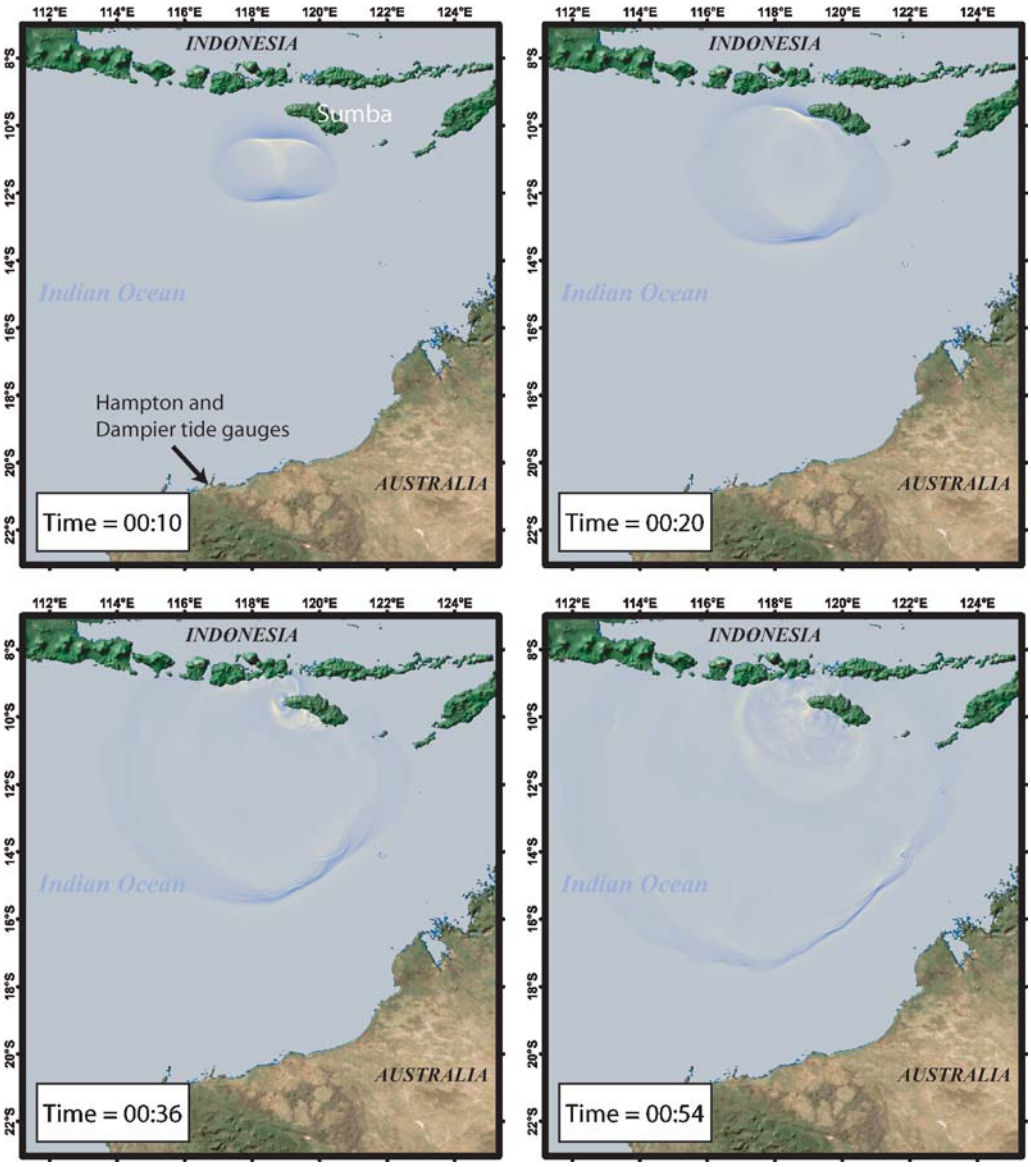

Figure 6. Snapshots of tsunami propagation at time = 10, 20, 36, and 54 min.

(D/L) is about 0.045, which is small enough to be able to assume that the sea surface deformation is the same as the ocean bottom deformation.

Results

Waveform Analysis and Tsunami Propagation

The comparison of the observed and computed tsunami waveforms for the great 1977 Sumba earthquake is shown in Figure 2. Because the first tsunami waves that arrived in Dampier and Hampton cannot be observed clearly, we used the later phase of the tsunami for the comparison and fitting. Tsunami simulation shows that the tsunami recorded at Port Hampton can be explained with slip amounts ranging from 3 to 7 m. This shows that the simulated tsunami on the later phase at this location is not changed significantly by the slip amounts although the first calculated tsunami waves at this station are increased when the slip amounts increased. The bathymetry and physiography offshore Dampier and Hampton are complex (Fig. 3). The nonlinear effect of tsunami propagation with this complex bathymetry makes the calculated tsunami on the later phase not linear to the slip amount. The tsunami numerical simulation result at Port Hedland, which has a simpler bathymetric feature, shows that only a 3 m slip amount can generate an acceptable tsunami amplitude (Fig. 2c). The tsunami propagates for about 20 min before it hits Sumba Island. After the tsunami hit Sumba Island, the tsunami was reflected by the island and propagated to the west and south directions (Fig. 6). The reflected tsunami wave that travels to the south may be one of the reasons why the tide gauge records at Hampton and Dampier show a high tsunami on the wave's later phase (Fig. 2). The other reason may be the edge waves occurred along the coast near Dampier.

Tsunami Inundation

The tsunamis computed from slip amounts between 3 and 7 m can explain the recorded tsunami from the two tide gauges at Dampier and Hampton. Thus, we run the tsunami inundation model with four slip amounts of 1, 3, 5, and 7 m to find the best model to explain the run-up of 8 m and inundation limit of 500 m at Lunyuk. The crustal deformation calculated from the slip amount of 1 m generates too small of a tsunami with inundation distance only around 100 m inland within the profiles I–L (Fig. 5). The deformation calculated from the slip amount of 5 m generates a tsunami within the

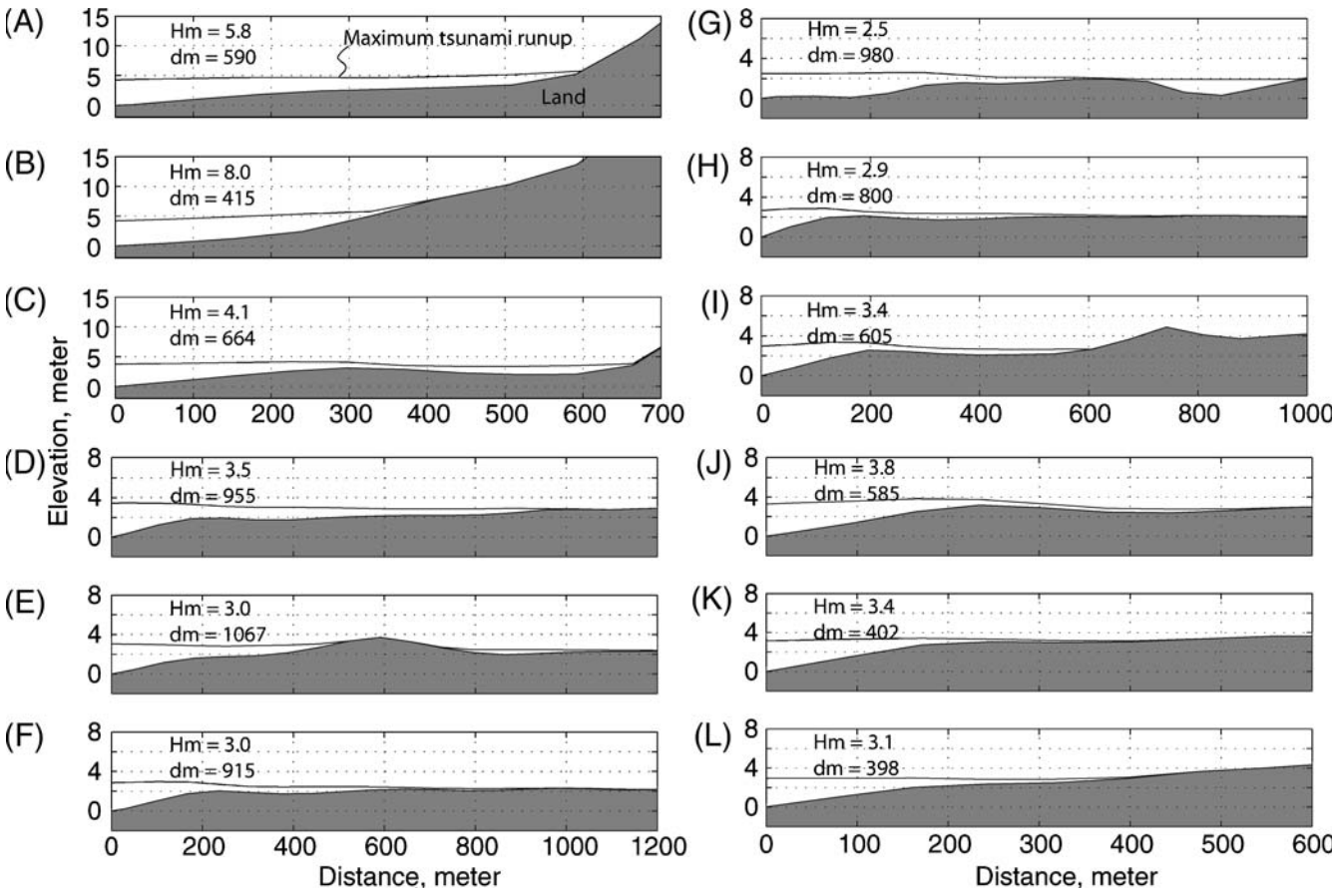

Figure 7. Inundation profiles in Lunyuk Bay; the solid line is the calculated maximum tsunami run-up along the profile, and the gray area is land. Hm is the highest tsunami run-up within the profile while dm is the distance from the coastline to the limit of inundation. Locations of those profiles (A–L) are shown in Figure 5.

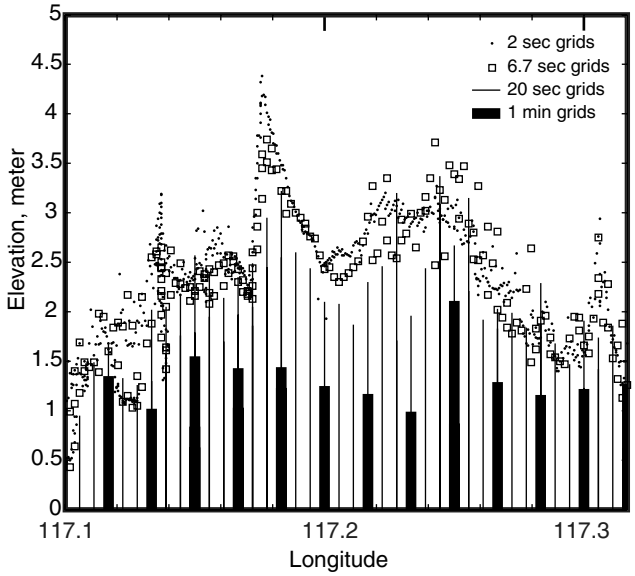

Figure 8. Comparison of the calculated maximum tsunami heights using the different grid sizes of 1 min (thick bar), 20 sec (thin bar), 6.7 sec (squares), and 2 sec (dots) along the coastline of Lunyuk Bay.

range of observed run-up (5–8 m); however, the maximum inundation distance of 2 km on the topography lows around the river is too long. The calculated inundation area shows that the deformation calculated from the slip amount of 7 m generates a maximum run-up of 15 m and an inundation distance of more than 2 km, which is way beyond the measurement. The observed tsunami run-up and inundation at Lunyuk are explained well by the computed tsunami from the slip amount of 3 m.

The highest run-up of 8 m and inundation distance of 415 m is generated along profile B. On profiles J, K, and L, which we suspect to be the location of the village affected by the tsunami, the simulated tsunami run-up ranges from 3.1 to 3.8 m and the inundation distance ranges from 398 to 585 m (Fig. 7), which is consistent with the reported inundation of 500 m. The longest inundation distance of 1.1 km along profile E is generated on topography lows with a mild slope along a meandering river (Fig. 5). The vertical sea deformation generated by the earthquake that best fit the tsunami inundation at Lunyuk is shown in Figure 1.

The tsunami numerical simulation usually underestimates the tsunami height when we use a coarse grid system such as a 1 min grid system. Satake and Tanioka (1995) show that computed tsunami heights using 6 sec grids can be twice as large as those on the 1 min grids for the 1993 Hokkaido Nansei-Oki tsunami. A detailed tsunami inundation model with high accuracy of bathymetry and topography data can generate tsunami run-up closer to observation. We compared tsunami heights at Lunyuk Bay computed using the nonlinear shallow water equation on different grid sizes, 1 min (1850 m), 20 sec (611 m), 6.7 sec (203 m), and 2 sec (68 m). To compare tsunami heights computed from different grid sizes, we calculated mean tsunami heights on the coastline (Fig. 8). The means of the calculated tsunami heights on the 2 sec grids are 1.0, 1.1, and 1.9 times larger than those on the 6.7 sec, 20 sec, and 1 min grids, respectively. The maximum tsunami heights along the coastline calculated using the 2 sec, 6.7 sec, 20 sec, and 1 min grid systems are 4.4 m, 3.7 m, 3.4 m, and 2.1 m, respectively. The maximum tsunami height computed using the 2 sec grid is about 2 times larger than the maximum obtained from the 1 min grid.

Larger run-up heights are mostly responsive to local topography, and if we do not use a small grid size, large run-up cannot be reproduced by numerical computation. The ratios of the observed run-up heights (5–8 m) to the calculated maximum tsunami height along the coastline, called the amplification factor, on different grid sizes are 1.1–1.8 for a 2 sec grid, 1.3–2.1 for a 6.7 sec grid, 1.5–2.4 for a 20 sec grid, and 2.4–3.8 for a 1 min grid (Table 2).

Conclusions

The three tide gauge records in Australia, the tsunami run-up of 8 m, and the inundation distance of 500 m in Lunyuk, Sumbawa, can be explained by the computed tsunami generated by the fault model with the slip amount of 3 m. Assuming the rigidity is between 6.0 and 6.8×10^{10} N m^{-2}, the range of the total seismic moment is calculated to be from 2.5 to 2.9×10^{21} N m (M_w 8.2). The seismic moment obtained from this study is similar to 2.4×10^{21} N m that was calculated by Silver and Jordan (1983) and slightly smaller than 4.0×10^{21} N m that was calculated by Given and Kanamori (1980). This study shows that the tsunami seismic moment is close to the traditional

Table 2

Numerical Calculation of Tsunami Heights along the Coastline of Lunyuk Using Different Grid Systems

Grid System	Mean of Calculated Tsunami Heights (m)	Maximum of Calculated Tsunami Heights (m)	Amplification Factor
2 sec	2.29	4.38	1.1–1.8
6.7 sec	2.28	3.74	1.3–2.1
20 sec	2.06	3.37	1.5–2.4
1 min	1.18	2.11	2.4–3.8

seismic moment; this means that the tsunami is generated by tectonic deformation rather than another tsunami generating force like a landslide (Abe, 1973). Comparison of the tsunami inundation model using different grid sizes shows that the average tsunami height on the coastline using a 2 sec grid is 2 times larger than using a 1 min grid system. The amplification factor for a 1 min grid system on Lunyuk Bay is 2.4–3.8, which may be used to roughly estimate the tsunami run-up within Lunyuk Bay.

Data and Resources

Digital bathymetry of 1 arcmin resolution used in this study can be obtained from General Bathymetric Chart of the Oceans at www.gebco.net (last accessed March 2009). We digitized the nautical charts of Dampier and Port Hedland supplied by the National Imagery and Mapping Agency. We digitized the nautical charts of Lunyuk Bay supplied by the Indonesia Navy (DISHIDROS-TNI-AL). The Shuttle Radar Topographic Mission (SRTM) digital elevation data of Lunyuk Bay used in this study can be obtained from http://srtm.csi.cgiar.org/ (last accessed March 2009). Tide gauge records in Australia were provided to us by Tony Lamberto, Department for Planning and Infrastructure, Australia.

Acknowledgments

This study was supported by the special coordination funds for promoting science and technology, "The Restoration Program from Giant Earthquakes and Tsunamis (Principal Investigator: Teruyuki Kato, Earthquake Research Institute, Univ. Tokyo)" by MEXT, Japan. We thank Cezar Trifu and two anonymous reviewers for their helpful comments and suggestions.

References

Abe, K. (1973). Tsunami and mechanism of great earthquakes, *Phys. Earth Planet. Interiors* **7,** 143–153.

Astiz, L., T. Lay, and H. Kanamori (1988). Large intermediate-depth earthquakes and the subduction process, *Phys. Earth Planet. Interiors* **53,** 80–166.

Chapple, W. M., and D. W. Forsyth (1979). Earthquake and bending of plates at trenches, *J. Geophys. Res.* **84,** 6729–6749.

Giardini, D. A., A. M. Dziewonski, and J. H. Woodhouse (1985). Centroid-moment tensor solutions for 113 large earthquakes in 1977–1980, *Phys. Earth Planet. Interiors* **40,** 259–272.

Given, J. W., and H. Kanamori (1980). The depth extent of the 1977 Sumbawa, Indonesia, earthquake, *EOS Trans. AGU.* **61,** 1044.

Imamura, F. (1996). Review of tsunami simulation with a finite difference method, in *Long-Wave Runup Models*, H. Yeh, P. Liu, and C. Synolakis (Editors), World Scientific, Singapore, 25–42.

International Tsunami Information Center (ITIC) (1977). Field survey of the tsunami of the 1977 Sumba earthquake, *Tsunami Reports*, 1977-12.

Kato, K., and Y. Tsuji (1995). Tsunami of the Sumba earthquake of August 19, 1977, *J. Nat. Disaster Sci.* **17,** 87–100.

Lynnes, C., and T. Lay (1988). Source process of the great Sumba earthquake, *J. Geophys. Res.* **93,** 13,407–14,320.

Mashinha, L., and D. E. Smylie (1971). The displacement fields of inclined faults, *Bull. Seismol. Soc. Am.* **61,** 1433–1440.

Robinovich, A. B., L. I. Lobkovsky, I. V. Fine, R. E. Thomson, T. N. Ivelskaya, and E. A. Kulikov (2008). Near-source observations and modeling of the Kuril Islands tsunamis of 15 November 2006 and 13 January 2007, *Adv. Geosci.* **14,** 105–116.

Ruff, L. J. (1996). Large earthquakes in subduction zones: Segment interaction and recurrence times (overview), in *Subduction Top to Bottom*, G. E. Bebout, D. W. Scholl, S. H. Kirby, and J. P. Platt (Editors), American Geophysical Union **96**, 91–104.

Satake, K. (2002). Tsunamis, in *Earthquake and Engineering Seismology*, W. H. K. Lee, H. Kanamori, P. C. Jennings, and C. Kisslinger (Editors), Academic Press, China, 437–451.

Satake, K., and Y. Tanioka (1995). Tsunami generation of the 1993 Hokkaido Nansei-Oki earthquake, *Pure Appl. Geophys.* **144,** 803–821.

Silver, P. G., and T. H. Jordan (1983). Total-moment spectra of fourteen large earthquakes, *J. Geophys. Res.* **88,** 3273–3292.

Spence, W. (1986). The 1977 Sumba earthquake series: Evidence for slab pull force acting at a subduction zone, *J. Geophys. Res.* **91,** 7225–7329.

Titov, V. V., F. I. Gonzalez, E. N. Bernard, M. C. Eble, H. O. Mofjeld, J. C. Newman, and A. J. Venturato (2005). Real-time tsunami forecasting: Challenges and solutions, *Nat. Hazards* **35,** 41–58.

Zhang, J., and H. Kanamori (1988). Source finiteness of large earthquakes measured from long-period Rayleigh waves, *Phys. Earth Planet. Interiors* **52** 56–84.

Institute of Seismology and Volcanology
Hokkaido University
Kita 10 Nishi 8 Kitaku
Sapporo 060-0810, Japan
(A.R.G., Y.T.)

Japan Agency for Marine-Earth Science and Technology
2-15 Natsushima
Yokosura 237-0061, Japan
(H.M.)

National Research Institute for Earth Science and Disaster Prevention
3-1 Tennodai
Tsukuba 305-0006, Japan
(S.-I.I.)

Manuscript received 4 November 2008